Chapter 3

Turbulence Model － Modification and Validation

This chapter focuses on the simulation of airfoil flows at pre-stall and stall conditions. Section 3.1 introduces briefly the features of stalled airfoil flow and the numerical difficulties to simulate them. A proposed modification based on the k-ε model is described in Section 3.2. The validation of the modified turbulence model is presented in Section 3.3 through comparing the numerical results with those from other models and the experimental data. A brief summary and conclusion are given in Section 3.4.

3.1 Stalled Airfoil Flow

As already mentioned in Chapter 1, airfoils at high angle of attack endure great geometry curvature and strong adverse pressure gradient near the nose. These lead to a large separation region directly behind the leading edge. Numerous small vortices exist in this so-called "dead-water" region. Beside the front separation, a separation region near the trailing edge may appear. The front separation causes a stall with sudden increases in the lift and drag fluctuations, while the rear separation has no serious fluctuation. At moderate Reynolds numbers between one thousand and one million, the airfoil flows in the vicinity of the leading edge are very sensitive to the initial transition point, location of separation, turbulence intensity near the separation, etc. These quantities, in turn, depend strongly on the airfoil geometry and Reynolds number.

For airfoils at high angle of attack, a stagnation point locates at the lower surface. Near the stagnation point, the turbulence will be suppressed. The streamlines will fit themselves to the wall and thus curve strongly. In the “dead-water” region upon the upper surface, the convection, molecular diffusion and turbulence have influences on each other in dependence of the Reynolds number.

The numerical difficulties on simulating such flow phenomena come from the fact that the turbulence models are generally developed for and extended from simple flows, e.g. the flows in ducts, channels or on plates. The parameters and constants are well constructed and validated for such flows. The turbulence models may, therefore, respond incorrectly on predicting complex flows. Even theoretically higher-order turbulence models seem to return to lower order when predicting airfoils at higher angles of attack. The k-ε model is the most widely used two-equation model in industrial applications. But it is known that

the standard k-ε model performs poorly on flows with impinging, separation, etc. and is unable to respond correctly to adverse pressure gradient. The model leads to poor prediction of the development of the boundary layer.

Many attempts have been made to improve the ability of the turbulence models. Kato and Launder proposed a modification of the production term of P_k in k and ε equations.[18] The modification uses strain and vorticity parameters to replace the conventional expression of the production term that uses only the strain parameter. Therefore, the turbulent kinetic energy is suppressed markedly near the stagnation point, while no effect has been made in simple shear flow. The modified turbulence model works successfully in predicting the flow over a square cylinder in which case forced separations occur at the edges. Jin and Braza proposed a similar modification on the term P_k.[16] Instead of using the product of strain and vorticity tensors, they recommended only a vorticity strain to simulate the term. This model has been applied to an airfoil flow of high Reynolds number and reasonable results have been obtained.

In this chapter, a modification considering the pressure gradient is introduced because certain incapability in predicting the airfoil flow at high angle of attack has been found with the known models. The modification is based on the Kato-Launder version because the over-prediction of the turbulent kinetic energy near the stagnation point is successfully suppressed. The detailed description and numerical validation of the modification are given in the following sections.

3.2 Modification of Turbulence Model

The production term in the k and ε equations is defined in Equation (2.28). It represents the rate of production of turbulent kinetic energy by the mean flow, and is responsible for the transfer of kinetic energy from the mean flow to the turbulence. This term needs to be closed before the partial differential equations are to be solved.

Usually, the production term is modeled by the eddy viscosity hypothesis as:

$$P_k = -\rho\overline{u_i'u_j'}\frac{\partial \bar{u}_i}{\partial x_j} = \mu_t\left(\frac{\partial \bar{u}_i}{\partial x_j} + \frac{\partial \bar{u}_j}{\partial x_i}\right)\frac{\partial \bar{u}_i}{\partial x_j}. \tag{3.1}$$

The suggested revision by Kato and Launder (hereafter KL model for short) can be written as:

$$P_k = -\rho\overline{u_i'u_j'}\frac{\partial \bar{u}_i}{\partial x_j} = \rho C_\mu \varepsilon S\Omega, \tag{3.2}$$

where S and Ω are dimensionless strain and vorticity parameters defined as:

$$S = \frac{k}{\varepsilon}\sqrt{\frac{1}{2}\left(\frac{\partial \bar{u}_i}{\partial x_j} + \frac{\partial \bar{u}_j}{\partial x_i}\right)^2} \quad \text{and} \quad \Omega = \frac{k}{\varepsilon}\sqrt{\frac{1}{2}\left(\frac{\partial \bar{u}_i}{\partial x_j} - \frac{\partial \bar{u}_j}{\partial x_i}\right)^2} \,. \tag{3.3}$$

They are equal in simple shear flow but differ from each other in complex flows.

The conventional modeling (referred to as NOR model) of the production term of (3.1) can be rewritten as

$$P_k = -\rho\overline{u_i' u_j'}\frac{\partial \bar{u}_i}{\partial x_j} = \rho C_\mu \varepsilon S^2 \,. \tag{3.4}$$

The modification on P_k from Kato and Launder brings reasonable results in a certain extent. But as can be seen later, the KL model fails to respond to adverse pressure gradient that emerges especially at the leading edge of the airfoil. The transition from laminar to turbulent, the separation point, and the development of the boundary layer cannot be captured correctly.

In this work, the KL model is further corrected using a dimensionless parameter f_p that includes the local pressure gradient, the turbulent kinetic energy and the dissipation rate:

$$P_k = C_\mu f_p \rho \varepsilon S \Omega \,, \tag{3.5}$$

where f_p and P_θ are:

$$f_p = \min\left(1, \frac{1}{P_\theta}\right) \tag{3.6}$$

$$P_\theta = \sqrt{\gamma \frac{\partial \bar{p}}{\partial x_i}\frac{\partial \bar{p}}{\partial x_i}}\frac{\sqrt{k}}{\rho\varepsilon} \tag{3.7}$$

$$\gamma = \delta_{ii} \,, \tag{3.8}$$

where δ_{ij} is the Kronecker symbol.

The parameter f_p corrects the production term in the flow field where its value is larger than unity. In a flow field with small f_p values, the production term will not be corrected.

The modification is based on the consideration that the turbulence behavior should be suppressed where large pressure gradient exists, either positive or negative. In airfoil flow, the large pressure gradient occurs mainly in the nose region and at the trailing edge where the flows from upper and lower surfaces begin to interblend. Indeed, because both the upper and lower boundaries of the computational domain are far from the airfoil surface, the airfoil flow simulated in this chapter is comparable with an external flow.

In the vicinity of the stagnation point, the flow is nearly irrotational. The turbulence is suppressed. However, the deformation of the fluid is enormous. The NOR model will encounter severe problem in this region. The overproduction of the turbulent energy will hinder the development of the flow downwards and predict a high level of mixing loss. The

KL model is ad hoc modification. It can suppress the excessive turbulent energy in the nose region. However, there is unphysical accumulation of turbulent energy in the boundary layer of the airfoil flow. The separation of the computed flow may be delayed by this effect. The predicted flow loss may be less than the real one. The WS model tries to correct the unphysical accumulation in the near wall region of the KL model. The dimensionless parameter includes two parts: the invariant of local pressure gradient and other local variables. There are certainly, many other possible parameter combinations. But the described one has been selected because it is proven to be able to give satisfactory results for separated airfoil flows.

In principle, the modification is oriented to the stalled airfoil that separates directly at the leading edge of the airfoil. However, to validate the ability of the modified model to various features of airfoil flow, the validation for the pre-stall angle of attack of 14 degrees of the $NACA63_3$-018 airfoil is also carried out. Results from the modified turbulence model and two other conventional models (with the Launder-Sharma near-wall resolution) are compared with the experiment al data, which is detailedly described in detail in Section 3.3.

3.3 Validation of Turbulence Model

The performance of the modified model on airfoil flows is investigated through comparing the results with the experimental measurement and the results from other turbulence models on an $NACA63_3$-018 airfoil at different angles of attack. The flows are under a chord-based Reynolds number of 300,000. The experimental data is provided by Prof. Hsiao of National Cheng Kung University in Taiwan. Their measurement was carried out in an open-type wind tunnel with a test section of $0.9\times1.2\,m^2$. An airfoil model of 305 mm in chord was used. Pressure distributions on both airfoil surfaces are available using wall pressure holes. Details about the experiment can be found in Shyu, Liu and Hsiao.[40][26][15] The experimental results are briefly summarized here.

The laminar boundary layer separates from the rear half of the suction side when the incidence angle is increased to 4 degrees. However, the flow remains attached on the pressure side of the airfoil. For higher angles of attack, a laminar boundary layer separation over the suction side moves upstream and remains laminar for a distance. It becomes then unstable and turns to be turbulent. At the angle of attack of 18 degrees, the pressure distribution on the suction side collapses suddenly. A precipitous decrease in lift and a large increase in drag indicate that the stall angle of the airfoil is 18 degrees.

In the following, the influence of grid quality is firstly investigated for the airfoil flow at the stall angle of attack of 18 degrees. The performances of different turbulence models on the same airfoil at 14 and 18 angles of attack are discussed thereafter.

3.3.1 Grid Investigation

The difficulties of RANS models lie in the prediction of the flow over a bluff body, such as an airfoil at high angle of attack, as the flow separates immediately from the leading edge of the airfoil. Sufficient resolution must be ensured. In this section, the influence of grid quality is discussed through comparing results from three computational grids with the same overall structure but different number of control volumes.

In the computation, the dynamic viscosity and density of the air are 1.8×10^{-5} kg/(m·s) and 1.2kg/m^3. The chord-based Reynolds number is 300,000. The inflow has a uniform velocity of 15.5 m/s with a turbulence of 0.25% according to the experiment. The Kolmogorov relation ($\varepsilon = k^{\frac{3}{2}} / l_\varepsilon$) is employed to estimate the dissipation at the inlet by specifying the length scale l_ε as a fraction of the characteristic inlet dimension, here the inlet height of 1.2 m.

The airfoil is set in the middle of the rectangular computational domain that has a height of 4 chords to simulate the test section in the wind tunnel and a width of 8.5 chords. The overall structure is schematically presented in 3.1. Five structured blocks are matched with each other to discretize the whole computational domain. The cells are mainly clustered at the leading and trailing edges of the airfoil. Near the airfoil surfaces and the wall boundaries, the grid is refined.

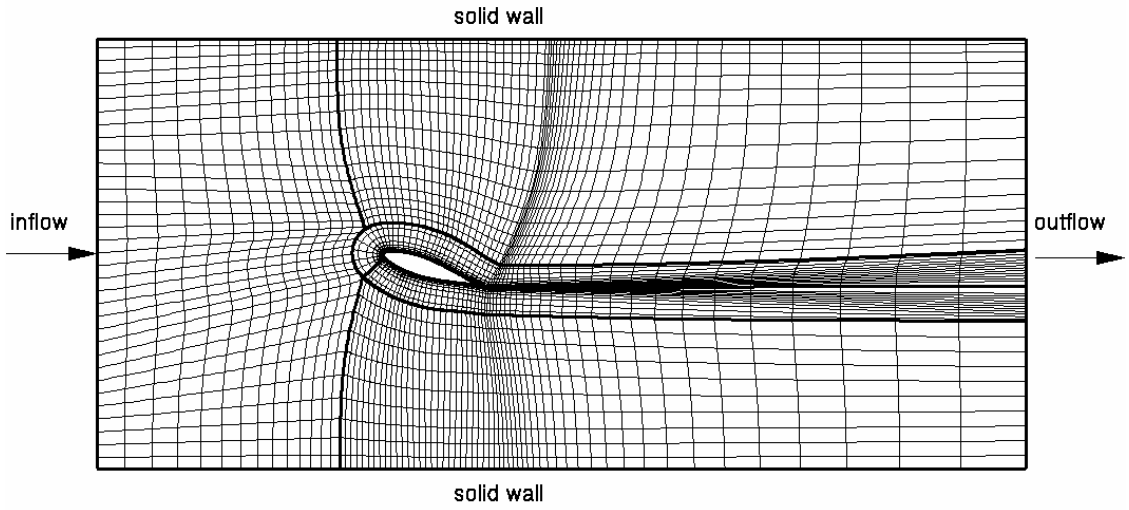

Fig. 3.1. Representative numerical grid for NACA63$_3$-018 airfoil at angle of attack of 18°, Re=300,000

The free stream velocity is set at the left side of the computational domain 2.6 chords upstream of the leading edge. An outflow condition of zero-gradient is imposed at the right

domain side 5 chords downstream of the trailing edge. Non-slip and impermeable conditions are imposed at the airfoil surface and both the upper and lower boundaries.

The convective fluxes are approximated using SMART scheme. The problem of pressure-velocity coupling is solved by SIMPLE method. The time step is advanced by implicit Euler method. SIP algorithm is the solver to the linear equation system. The accuracies for both velocity components and the pressure are 10^{-6}.

Three different grids are employed to compute the airfoil flow with the same conditions. They have 29,000 cells for the first grid, 54,000 for the second and 110,000 for the third one. The finest grid has 215 and 192 cells on the suction and pressure side of the airfoil, respectively, whereas the coarsest has 108 and 96 cells. The middle one has 149 and 116 cells.

In the investigation of grid quality, the new modified turbulence model described in Section 3.2 is applied. The near wall flow is resolved by the low-Reynolds-number modification proposed by Launder and Sharma (1974) that is described in Chapter 2.[21] The average y^+ values for the first grid lines around the airfoil are 0.7, 0.6 and 0.4 for the coarse, middle, and fine grid, respectively.

It is noteworthy that the computations are time dependent. The whole flow field tends to reach a steady state if there is enough time development. The flow quantities do not vary any more after certain time steps. The integral quantities as the lift and drag that will be discussed in this chapter are obtained from this stage. The obtained steady state is independent of the initial condition.

However, the development of the flow field rests on the given initial condition. Some quasi-periodicity may appear if the computation is started from a zero flow field (of velocity and pressure). The integral quantities, as the lift and drag of the airfoil, show an unchanged frequency. But the amplitudes of the quantities are decreased in each following period. The typical lift history of such a computation is schematically shown in Figure 3.2. Along with the attenuation of the amplitude, the lift approaches asymptotically to a constant value.

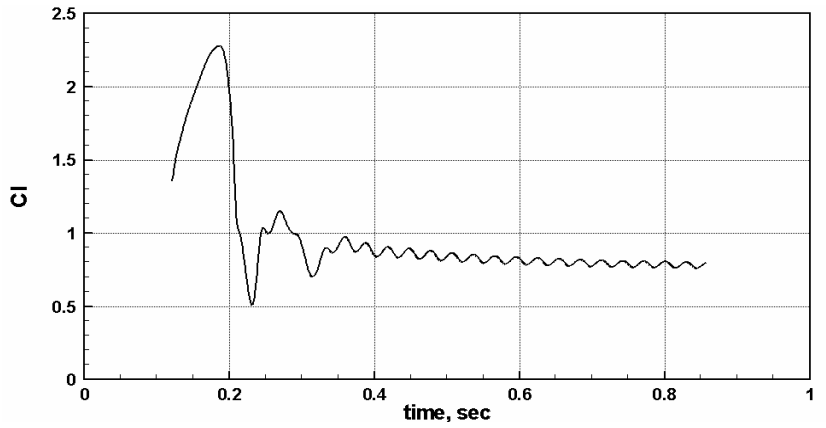

Fig. 3.2. Schematic representation of lift coefficient history for fine grid of NACA63_3-018 airfoil at 18 AOA, Re=300,000

The fact that the computational solution tends to become steady might rise from the approximation schemes. It is clear that many methods, including all upwind ones, are energy dissipative. They include as part of the truncation error a diffusive term that will dissipate energy in a time dependent calculation. The dissipation they introduce tends to stabilize numerical methods. When such methods are applied to the solution of steady problems, there is a kind of self-correction that keeps the numerical error from growing too large. In this work, their accumulated effect with time may also bring similar effects to the flow field, although the applied schemes for the time-independent terms have second order truncation errors. There is so far a lack of a systematic investigation on such effects. Additionally, it is considered that the imposing of a zero-gradient condition at the outlet of the computational domain may damp the periodicity of the flow phenomenon. Its integral effect with time makes the flow field becoming steady and the quantities of the flow field do not vary any more after some computation steps.

On the other hand, it is clear that the steady solution resulting from the unsteady computation fulfils approximately the discretized partial differential equations of RANS equations as the truncation error is of higher order. The steady solution is also reasonable. The average quantities are considered as the temporal averaged results of the flow field.

In this work, it is observed from the results of time-dependent computation that a regular vortex-shedding with fixed frequency exists in the procedure. Therefore, this frequency is referred to as the vortex-shedding frequency. The steady flow field is considered as a temporal average of the physical phenomenon along a large time interval. The integral quantities discussed in this work are all obtained from the unsteady computation.

In the computations for different grids, the time step is fixed to be 0.0005 second for the all three grids. The advancing time interval ensures that there are about 60 discrete time steps in each vortex-shedding procedure of the airfoil flow. It is considered to be enough to capture the right vortex-shedding frequency. The phase shift effect is not discussed in this work. A detailed investigation of the time discretization and its effect on the accuracy of the results can be found in Date and Turnock.[9]

Figure 3.3 gives the distributions of turbulent kinetic energy resulting from the grids. The turbulent kinetic energy is non-diemensionalized by the square of free stream velocity. It can be found that the grids provide qualitatively the same result. But quantitative differences exist.

The comparison of some characteristic quantities from different grids is collected in Table 3.1. These quantities are the separation position in percents of chord, the height of the large separation above the upper surface measured at the trailing edge (in multiples of chord), the maximal spreading width of 10% turbulence upright to the free-stream flow direction measured in multiples of chord, and the lift and drag coefficients.

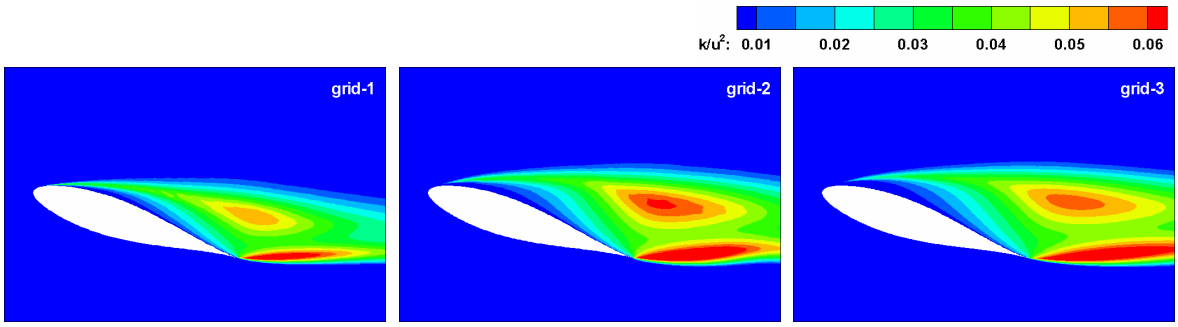

(a) (b) (c)

Fig. 3.3. Distribution of turbulent energy and flow pattern resulting from three computational grids for NACA63$_3$-018 airfoil at 18 AOA, Re=300,000

	Grid-1	**Grid-2**	**Grid-3**
Cell Number	29,000	54,000	110,000
average y^+	0.7	0.6	0.4
Separation Position (%C)	1.79	1.25	1.25
Separation Height (C)	0.32	0.40	0.41
Lift Coefficient C_l	0.927	0.740	0.665
Drag Coefficient C_d	0.260	0.290	0.279

Tab. 3.1. Comparison of results from three computational grids for NACA63$_3$-018 airfoil at 18 AOA, Re=300,000

It can be found that all of the three computational grids are able to reproduce the massive separation from the leading edge. The exact position obtained from the first (coarsest) grid has about 50% relative error with those from two other grids. The second grid is as exact as the third one in obtaining the separation point. The height of the separation region obtained by the first grid is 20% smaller than those from the other grids. Only 2% difference is observed between the second and the third grids. The results from the second grid have already approached very closely to those from the third grid.

The differences in the separation position and the characteristic dimensions result in the deviation for the integral quantities. The first grid overestimates the lift coefficient by 40% in comparison with the third grid. The second one has 11% difference. The drag coefficient obtained from the first grid is underestimated by 7% and overestimated by 4% from the second grid.

Figure 3.4 shows the distributions of pressure coefficient on the airfoil surfaces

obtained from all the grids. The coefficient is non-dimensionalized by $\frac{1}{2}\rho u_\infty^2$. From the first grid results a large suction peak on the upper airfoil surface, although it can reproduce the separation position qualitatively. In comparison, the pressure distributions from the second and third grid have only small distinction on the front half of the airfoil.

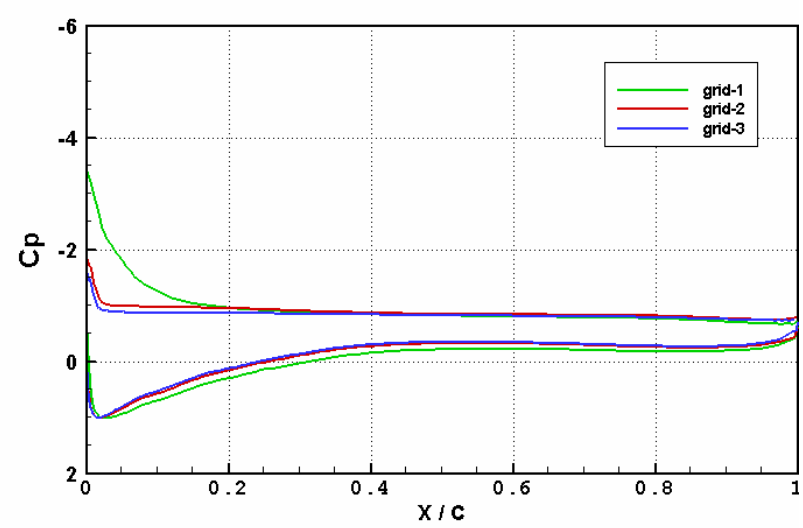

Fig. 3.4. Comparison of pressure distribution on airfoil surfaces obtained from three computational grids for NACA63_3-018 airfoil at 18 AOA, Re=300,000

It can be obtained from above analysis that the refinement of the computational grid has large influence on the numerical result, especially on the lift and drag coefficients. The determination of the separation point and the grid denseness in its vicinity are the crucial guidelines for the grid quality. The coarse grid has difficulty in reproducing the pressure distribution in the separation region and hence, is only capable of providing qualitative results. Because the results from the second and third girds differ little from each other, it can be concluded that the third grid has enough spatial resolution to the flow. The integral quantities may have the error within few percents.

The computational results that will be discussed below are obtained from the same manner of discretizations for the finest grid. For different angles of attack, the grids are slightly changed to adapt to the angle shifts of the airfoil. But the grid structure and the overall cell number are not modified.

3.3.2 Angle of Attack of 14 Degrees

The performance of the modified turbulence model on the airfoil at pre-stall condition is validated through computing the NACA63_3-018 airfoil at an angle of attack of 14 degrees, at which the airfoil can remain higher lift and lower drag and the flow separates laminarly

at the mid portion of the airfoil.

The distribution of P_θ defined in Equation (3.7) is shown in Figure 3.5. In the flow field away from the airfoil surfaces, the value of P_θ is less than unity. The production term will not be corrected. The parameter P_θ is of higher level near the vertex above the upper airfoil surface and reaches the maximum at the leading and trailing edge.

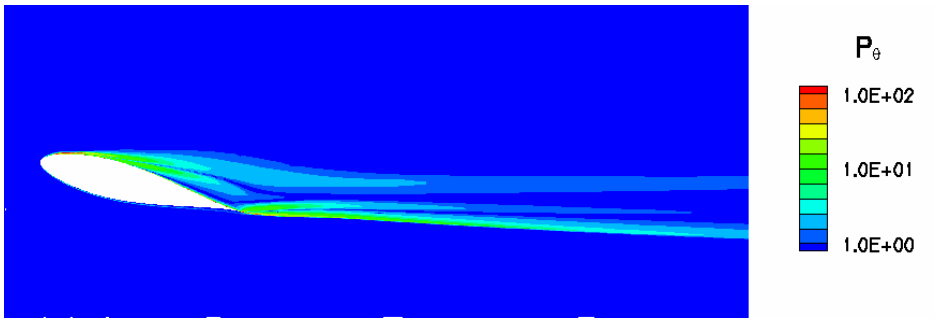

Fig. 3.5. P_θ distribution for NACA63$_3$-018 airfoil at 14 AOA, Re=300,000

Figure 3.6 gives the distributions of turbulent kinetic energy around the airfoil and the corresponding flow patterns resulting from the turbulence models. The turbulent kinetic energy is made dimensionless by u_∞^2.

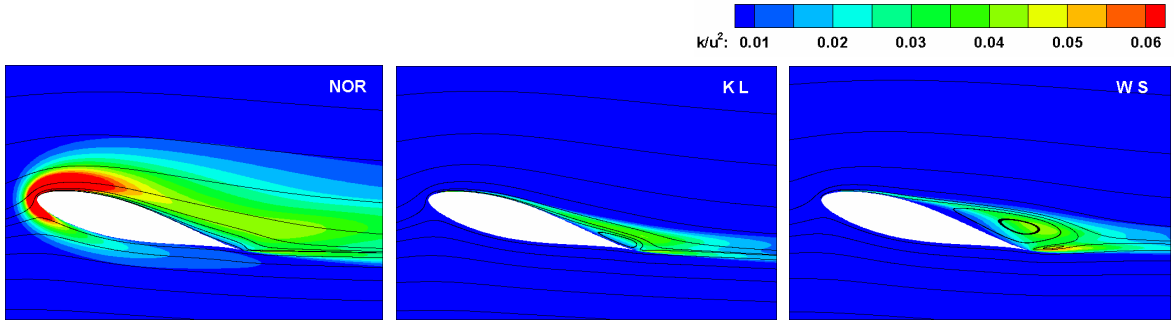

(a) (b) (c)

Fig. 3.6. Distribution of turbulent energy and flow pattern obtained from NOR, KL and WS models for NACA63$_3$-018 airfoil at 14 AOA, Re=300,000

Figure 3.6(a) shows the result of NOR model. The turbulence is of higher level around the whole airfoil. At the leading edge, a turbulence of higher than 80% is obtained and extends to 0.4 chords downstream where the turbulence is defined by $T_u = \sqrt{k}/u_\infty$. The turbulent kinetic energy is suppressed by the adverse pressure gradient downstream of the leading edge. The turbulence in the boundary layer is less energetic on the rear half of the suction side than its value upstream. The development of the boundary layer is influenced

by the overproduction of the turbulent kinetic energy and no separation is predicted by this model. The streamlines diffuse themselves at the trailing edge. The turbulent energy extends about 4 chords downstream of the trailing edge in the wake.

The KL model reduces markedly the turbulent kinetic energy at the leading edge and near the stagnation point, as can be seen in Figure 3.6(b). This is because the KL model takes the product of the strain and vorticity to model the generation of the turbulent energy in the leading-edge region where the flow is nearly irrotational. It can be said that the KL model is successful in the front region of the airfoil flow. However, the generation is not improved at all when the flow passes over the maximal height of the airfoil in the field as the flow is under the effects of adverse pressure gradient and geometric curvature. The magnitudes of the production term differ little between the NOR and KL descriptions. A separation bubble with a length of 0.04 chords accomplishes the transition whose onset locates at 2% chord on the suction side of the airfoil. The bubble is about 0.1mm height. The turbulence is higher than 10% in the boundary layer downstream of the separation bubble, except in the sub-layer region. The flow separates turbulently at 71% chord. The flow of 10% turbulence extends one chord downstream of the trailing edge.

The distribution of the turbulent kinetic energy at the leading edge obtained by WS model is similar to that from KL model, as can be seen in Figure 3.6(c). A separation bubble with its front at about 0.024 chords induces the flow transition. The length of the bubble is about 0.1 chords, which is 2.5 times the bubble length predicted by KL model. The outer region of the boundary layer downstream of the separation bubble remains turbulent until the flow separates again at 38% chord. The prediction of separation position agrees well with the experimental data of 51% chord, although an error of 0.1C exists between them. The experimental separation point should be delayed in certain extend because the hot wire, which was employed in the experiment to detect the reverse flow, cannot be placed closely to the wall.

The profiles of streamwise velocity at seven chord positions from 0.1 to 0.7 chords obtained from all the three turbulence models are presented in Figure 3.7. The ordinate is the dimensionless vertical distance to the origin measured in multiples of chord. The experimental data are represented by black dots. The numerical results from NOR, KL and WS model are denoted by green, red and blue lines, respectively. It can be observed that in the outer region of the boundary layer, results from all the turbulence models are in good agreement with the experimental data. The velocity recovery predicted by KL model is slightly delayed in the region of large geometric curvature. In the boundary-layer region, the turbulence models behave quite different. At 0.1C of the geometric vertex, the KL and WS model seem to underestimate the turbulent kinetic energy. The velocity is higher than the experimental data. The NOR model saturates the velocity profile in the inner layer of the boundary. But in the outer layer, the velocity is lower than the experimental data as the high level of turbulent kinetic energy induces intensive momentum exchange. The local zoom-in picture of the velocity profile at 0.1C is given in the lower left corner.

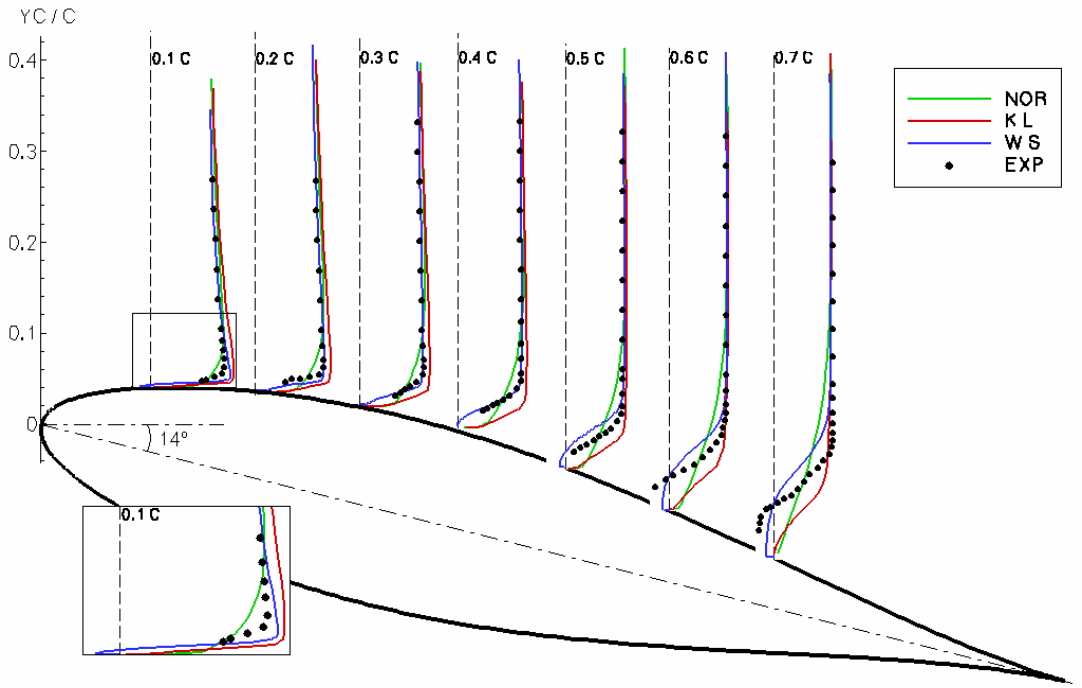

Fig. 3.7. Comparison of velocity profiles obtained from NOR, KL, WS models and experiment for NACA63_3-018 airfoil at 14 AOA, Re=300,000

Downstream of the location of 0.1C, the velocity profile predicted by NOR model becomes more acclivitous as a result of the decrease of the turbulent energy inside the boundary layer. The flow retains fully attached on the surfaces and no separation has been found in the whole flow field. The decrease of the turbulent energy also sharpens its velocity profile. The KL model finds the separation at 71% chord. Before the separation region, velocity disparity has been observed between the results from the KL model and the experimental data.

In opposition to the incapability of the NOR and KL models to predict the massive separation, the WS model shows its feasibility to such flows. The computational results of the velocity profile obtained from WS model agree quite well with the experimental data. The model predicts a separation bubble between 0.2% and 1.2%C through which the transition of the flow accomplishes. Downstream of the separation bubble, the turbulence is about 20%. The turbulent kinetic energy concentrates mainly in the boundary layer and disperses due to geometric curvature. Before 0.4C, the results from WS model are nearly identical with the experimental data. It predicts a separation at 38% chord, which is about 0.1C of the experimental result of 51% chord. Downstream the separation point, a recirculating region is formed above the upper airfoil surface, together with a trailing-edge separation that extends about 0.15 chords in the wake. The velocity of the reverse flow near the wall is underestimated by WS model and the velocity restoral is also deferred. But in principle, the WS model can qualitatively reproduce the important flow features that

occur at pre-stall angle of attack.

Given in Figure 3.8 is the comparison of pressure distribution along the airfoil surfaces between numerical and experimental results. The pressure is expressed in dimensionless form by $\frac{1}{2}\rho u_\infty^2$. The NOR model has difficulties in predicting the stagnation-point pressure as the pressure coefficient is 1.28. Downstream of the stagnation point on the pressure side of the airfoil, all the NOR, KL and WS turbulence models have good accordance with the experiment. In the vicinity of the leading edge on the upper surface of the airfoil, results from NOR and WS models have small difference with the experimental data. Downstream of 0.1C, very good conformity between the numerical results obtained from WS model and the experimental data has been found, whereas the results from NOR and KL models cannot reproduce the experimental data from about 0.2C downstream of the airfoil. It can be summarized that the NOR, KL and WS models can qualitatively reproduce the pressure distribution along the airfoil surfaces, whereas a better agreement with the experimental data is achieved by the WS model.

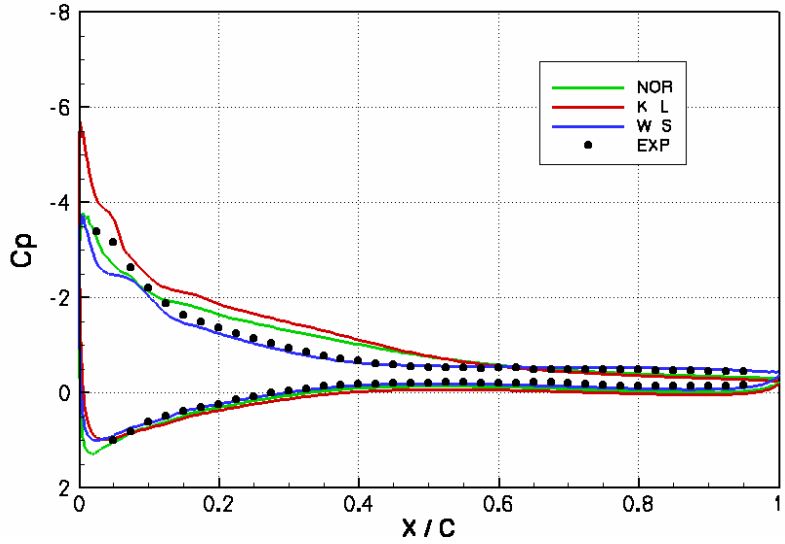

Fig. 3.8. Comparison of pressure distribution on airfoil surfaces obtained from NOR, KL, WS models and experiment for NACA63_3-018 airfoil at 14 AOA, Re=300,000

Tabulated below are the lift and drag coefficients and other flow features from NOR, KL and WS models, together with the experimental data. It can be found that the result of lift from NOR model is 22% higher than the experimental data, while the value from KL model is even 41% higher. The NOR model predicts a drag 50% higher than the experimental data, the KL model 26% lower. In contrast, the results from WS model are in close conformity with the experimental data. Less than 2% relative errors in lift and drag are found. The WS model also predicts a reasonable result for the separation point of the flow. It is stated in the experiment that the reverse flow is found at 51% chord. This would

be slightly delayed as the streamwise velocity is detected through the hot wire and the lack of experimental data is quite possible. The KL model finds a reverse velocity at first at 71% chord, whereas the NOR model is not able to reproduce any separation at all. Additionally listed below are the extending length of 10% turbulence of the flow in the wake and the spreading width of 10% turbulence at 0.5 chords downstream the trailing edge, etc.

	NOR	**K L**	**W S**	**EXP**
C_l	1.156	1.342	0.948	0.95
C_d	0.180	0.089	0.117	0.12
Sep. Bub. (%)	---	2-6	3-12	?
Turb. Sep. (%)	---	71	38	~51
Turb. wake (C)	4.0	1.1	1.5	?
Turb. width (C)	0.5	0.1	0.1	?

Tab. 3.2. Comparison of numerical and experimental data for NACA63_3-018 airfoil at 14 AOA, Re=300,000

It can be summarized from above comparison and discussion that for the airfoil at moderate angle of attack at which the flow separates at the mid portion of the airfoil, different results can be obtained from different turbulence models. The NOR model has the known problem of predicting excess turbulent kinetic energy in the vicinity of the leading edge which comes from the fact that the model closes the Reynolds stress through mean deformation of the flow. The deformation would be enormous near the stagnation point and around the airfoil nose where the streamlines are curved strongly. The overproduction of the turbulent energy at the leading edge leads to extra flow losses and the development of the boundary layer is strongly influenced by this effect. Therefore, it is normal that the integral quantities as the lift and drag of the airfoil obtained from NOR model deviate considerably from the experimental data.

The overproduction of turbulent kinetic energy at the leading edge is corrected by KL model in a certain extent. But the recovery of streamwise velocity is delayed and a late separation at 71% chord is found. In contrast, the WS model can reproduce the flow in a large extent in comparison with the experimental data and reliable results as the lift and drag are obtained.

It can be concluded that the WS model is applicable to airfoil flows at moderate angles of attack. Further validation of the turbulence model on the same airfoil at stall angle of 18 degrees is presented below.

3.3.3 Angle of attack of 18 Degrees

It is quite difficult to simulate the massive separation on the stalled airfoil using RANS equations because the separation of this kind is very sensitive to the flow features as the turbulence, the Reynolds number, the onset of transition, etc. In this section, the performances of different turbulence models on the stalled NACA63_3-018 airfoil are compared and discussed.

The simulation conditions are set the same as those for the angle of attack of 14 degrees, including the fluid properties as the density, dynamic viscosity, the free-stream velocity and its turbulence, and the numerical considerations as the approximation schemes, solution methods and the accuracy. The computational grid has the same structure as that one used for the case of 14 AOA. The number of the cells that discretize the entire computation domain is also the same.

Depicted in Figure 3.9 is the distribution of parameter P_θ for the airfoil at the stall angle of attack. Similar to Figure 3.5, the outer flow region far from the separation has the value of P_θ less than unity and is not revised by the WS model. The modification concentrates mainly on the leading-edge region near the geometric vertex and the trailing edge where the flows from the upper and lower surface begin to interact.

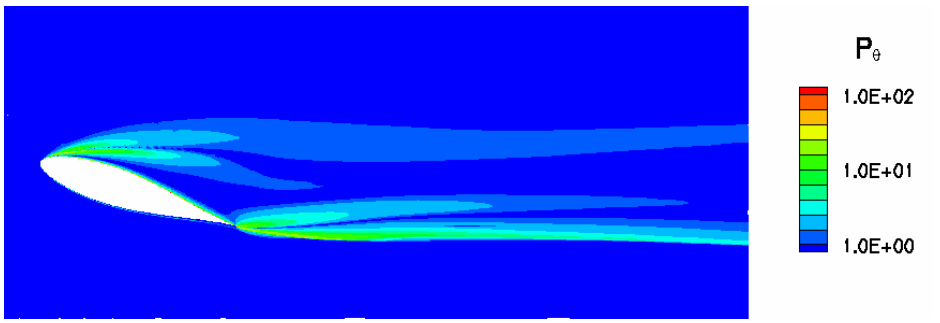

Fig. 3.9. P_θ distribution for NACA63_3-018 airfoil at 18 AOA, Re=300,000

Given in Figure 3.10 are the distributions of turbulent kinetic energy and flow patterns obtained from (a) NOR, (b) KL and (c) WS model. The turbulent kinetic energy is made dimensionless by u_∞^2. Resembling the Figure 3.6(a), the turbulent energy and its dissipation obtained from NOR model remain of high level in the nose region of the airfoil. The flow above the suction side of the airfoil is fully turbulent. Near the leading edge, the turbulence of higher than 40% and a very thick layer around the leading edge with 20% turbulence is found by this model. The flow has more resistance to separation because of the intensive momentum exchange in the near-wall region. A late separation at 51% chord is detected without rear separation. One can find that the NOR model is unable to predict

the stalled airfoil flow undergoing large geometry curvature and strong adverse pressure gradient.

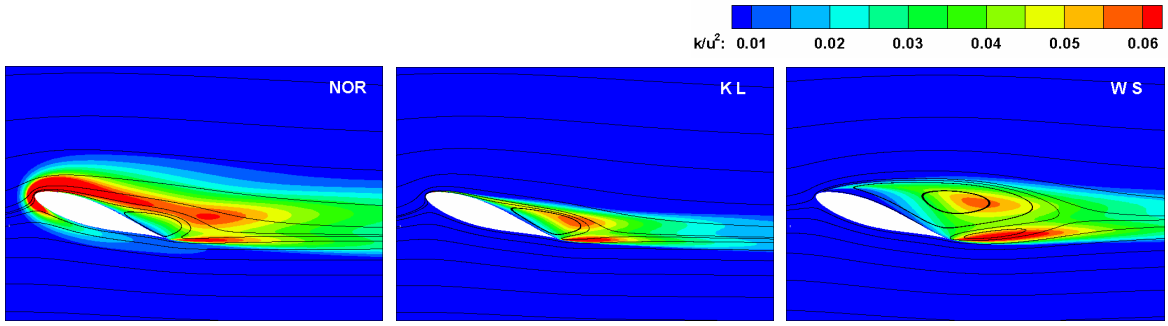

(a) (b) (c)

Fig. 3.10. Distribution of turbulent energy and flow pattern obtained from NOR, KL and WS models for $NACA63_3$-018 airfoil at 18 AOA, Re=300,000

Figure 3.10(b) gives the distribution of turbulent kinetic energy and flow pattern obtained from the KL model. The turbulence is less than 1% near the stagnation point and at the leading edge. The over-production of turbulent kinetic energy in these regions is suppressed. Nevertheless, because the deformation at the leading edge is enormous, the turbulent kinetic energy in the vicinity where the real flow tends to separate is also very high. The turbulence stays over 20% near the experimental separation point and 10% over the suction side, except in a thin layer near the wall. Through the onset of the transition near 3% chord on the suction side, the flow turns to be turbulent. A separation is obtained at 47% chord from this model.

The distribution of the turbulent kinetic energy and flow pattern predicted by WS model are shown in Figure 3.10(c). The leading and trailing-edge separations are found. At the leading edge, the flow separates at 1.2% chord on the suction side. Upstream of the separation point, the turbulence is less than 1%, which implies a laminar separation for the stalled flow is obtained. Downstream of the separation, the turbulence grows up rapidly. At about 5% chord, the turbulence reaches 5%. It reaches 10% at 10% chord. The turbulence is over 20% at the cores of the large separation region.

From above discussion, it can be summarized that the WS modification is the most accurate model to predict airfoil flow with massive separation in the sense of reproducing the start point for the separation. Further comparison of the pressure distribution is shown in Figure 3.11 in which the results from NOR, KL and WS models are drawn with different colors, together with the experimental data denoted by dots. The pressure is non-dimensionalized by $\frac{1}{2}\rho u_\infty^2$.

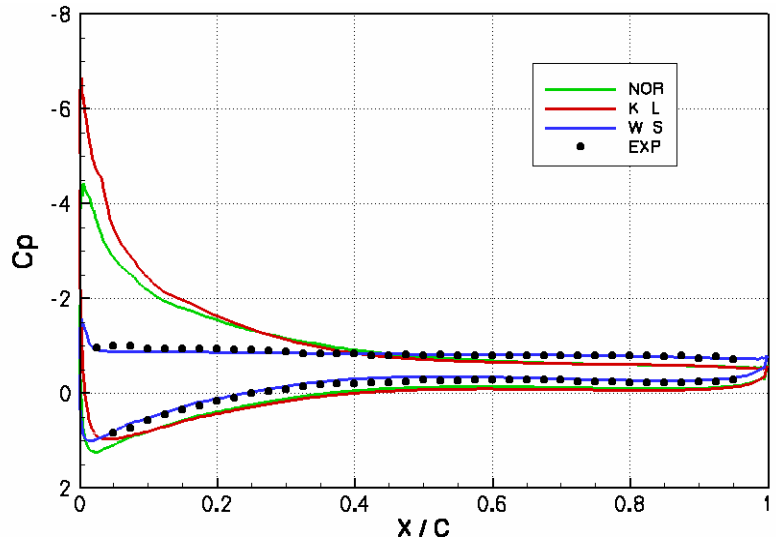

Fig. 3.11. Comparison of pressure distribution on airfoil surfaces obtained from NOR, KL, WS models and experiment for NACA63_3-018 airfoil at 18 AOA, Re=300,000

The pressure distributions resulting from NOR and KL models vary only a little from their values for the airfoil at the angle of attack of 14 degrees. A higher suction peak of –4.4 from NOR and –6.4 from KL model exists on the suction side of the airfoil surface. Again, the NOR model fails to predict the pressure at the stagnation point and hence the development of the boundary layer on the pressure side of the airfoil deviated greatly from the experiment. The KL model has few problems on the stagnation point, but the pressure is overestimated on the lower surface of the airfoil, like the situation with NOR model. The distance of the pressure distribution between the NOR, KL models and the experiment stems from the underestimation of the velocity recovery in the boundary layer by the two turbulence models.

The comparison shows that both NOR and KL models are not sensitive to the shape modification downstream of the geometric vertex of the airfoil in the flow field and hence, unable to reproduce the pressure distributions on the airfoil surfaces that are important for determining the aerodynamic performance.

In contrary, the pressure distribution on both surfaces of the airfoil obtained from WS model accords extremely well with the experimental data. The pressure at the stagnation point is well captured and the pressure plateau is also well reproduced.

Table 3.3 lists in detail some numerical results from the NOR, KL and WS models, together with experimental data. The lift and drag are given in dimensionless form by referring them to $\frac{1}{2}\rho u_\infty^2$. The lift coefficients from NOR and KL models have 80% and 97% deviations from the experimental data, respectively, while the corresponding drag coefficients have 11% and 46% differences with the experimental data.

	NOR	K L	W S	EXP
C_l	1.203	1.319	0.665	0.67
C_d	0.267	0.162	0.279	0.30
Sep. (%)	47	51	1.2	~1.25
Turb. wake (C)	> 4.9	2.9	4.5	?
Turb. width (C)	0.6	0.2	0.5	?

Tab. 3.3. Comparison of numerical and experimental data for NACA63_3-018 airfoil at 18 AOA, Re=300,000

It can be concluded from above discussion that the NOR and KL model are not able to reproduce the airfoil flow at stall angle of attack. The massive separation is delayed to the mid portion of the airfoil by both models. The aerodynamic performances are not correctly predicted. The two models perform quite poorly on airfoils with leading-edge separation. On the contrary, the results from WS model show much better agreement with the experimental data, including the lift, drag, the separation point, etc. All the important engineering quantities are well reproduced. The WS model is applicable for airfoil flows at high angles of attack.

3.3.4 Conclusion

The airfoil flow under moderate Reynolds number is very sensitive to the subtle change of the geometry, especially in the vicinity of the leading edge. The numerical results may differ considerably from the experimental data with different models. The turbulence model is the crucial factor to the computational outcome. In this section, the performances of three turbulence models are investigated on an NACA63_3-018 airfoil at angles of attack of 14 and 18 degrees. The chord-based Reynolds number is 300,000.

For the pre-stall angle of attack of 14 degrees, the NOR model produces a high level of turbulent energy around the airfoil, especially in the nose region. The enhanced momentum exchange in the near-wall region enables the flow remaining unseparated in the flow field. As a result, the pressure on the airfoil surfaces deviates greatly from the experimental data. Accordingly, the airfoil lift and drag cannot be predicted reasonably.

The KL model modifies the production term in such a way that the suppression of the high level of turbulent energy around the leading edge is achieved. Near the stagnation point, the flow resolution is improved. However, the velocity recovery is slightly delayed after the flow turning over the leading edge of the upper surface. The high level of turbulent energy and dissipation is found in the inner layer of the boundary near the geometric vertex, which turns on the transition of the flow to become turbulent. The

separation point is, therefore, difficult to agree well with the experimental data.

The WS model, which is based on the KL modification, corrects further the production in the region where strong pressure gradient exists. Results show extremely good agreement with the experimental data, including the integral quantities as the lift and drag, the streamwise velocity, etc. The comparison indicates that the WS model is much more reliable than other models in predicting airfoil flow at pre-stall angles of attack.

At stall angle of attack, a precipitous decrease in lift and a large increase in drag appear. The NOR model again, obtains the flow with high level of turbulent energy around the airfoil nose and destroys the development of the boundary layer. The predicted separation point has large deviation from the experimental data. The lift and drag have large relative error. The NOR model is not appropriate in predicting the massive separation.

Results from KL model are not better than those from NOR model. The KL model predicts high level of turbulent energy and dissipation at the geometric vertex where the transition is induced by this effect. Downstream, the turbulent energy remains very high in the near-wall region. The flow separates at the mid portion of the airfoil. The lift and drag have large relative error in relation to the experimental data. Therefore, the KL model is unable to predict stalled airfoil flow, either. It is not sensitive to the change of angle of attack.

The best results come from the WS model. It obtains the separation point at 1.2% chord, which is nearly identical with the experimental result. The feature of pressure plateau on the upper surface is also well captured. The results ensure the competence of the WS model in predicting the aerodynamic performance of the stalled airfoil.

In short, the WS model responds properly to the change of angle of attack of the airfoil and performs well on predicting the integral quantities of engineering interest. It is suitable for airfoil flows at pre-stall and stall angles of attack.

3.4 Closure

The topics in this chapter are around the turbulence model. First of all, the influence of grid quality is investigated for an NACA63_3-018 airfoil at an angle of attack of 18 degrees using three grids with different numbers of control volumes. Results show that for stalled airfoil flow that separates directly at the leading edge, enough cells must be clustered near that region to ensure the resolution. Large error may occur if a coarse grid is employed.

As no known models can adequately resolve the massive separation, a modification to the k-ε model is introduced. The performance of the modified model is investigated for an NACA airfoil at pre-stall and stall angles of attack. Numerical results from the model are compared with those from two other accustomed models and the experimental measurement. It has been shown that the modified turbulence model reproduces quite good results, including the separation position, the lift and drag of the airfoil, etc., in comparison

with experimental results. The other models are not sensitive to the variation in the angle of attack of the airfoil and are not reliable in providing the aerodynamic performances of the airfoil.